Two-Dimensional Singular Vector Elements for Finite-Element Analysis

Zorica Pantic-Tanner, J. Scott Savage, *Student Member, IEEE,* David R. Tanner, *Member, IEEE,* and Andrew F. Peterson, *Senior Member, IEEE*

***Abstract*— The finite-element method (FEM) exhibits a reduced convergence rate when used for the analysis of geometries containing sharp edges where the electromagnetic field is singular. The convergence of the method can be improved by introducing singular elements that model analytically predicted singular behavior. A number of authors have developed singular elements that are compatible with the scalar FEM. In this paper, we propose a new singular element that is compatible with edge-based vector finite elements and can cope with any order of singularity while preserving the sparsity of the FEM equations. Edge-based singular elements more correctly model singular fields and thus require fewer unknowns, while avoiding the introduction of spurious modes in the numerical solution. Numerical results verify that the convergence of the FEM is significantly improved.**

***Index Terms*—Finite elements, munerical analysis.**

I. Introduction

THE FINITE-ELEMENT method (FEM), based on vector or edge elements, is a powerful numerical technique for solving a variety of waveguide and cavity problems. It is capable of handling isotropic or anisotropic inhomogeneous media, and it suppresses nonphysical spurious modes from the numerical solution. However, many of these structures contain conducting or dielectric edges, and the field behavior can be singular in the vicinity of these edges [1], [2]. If traditional polynomial edge elements are used to model these rapidly varying fields, it becomes necessary to use a fine mesh in the vicinity of the edge [3], [4]. This is despite the observation that ordinary edge elements are better suited than scalar expansions for coping with the singular field behavior, since the normal field component is allowed to be discontinuous at a sharp edge [5], [6]. The additional unknowns in the mesh increase the computational time as well as memory requirements [7]. One proposed remedy is to augment the trial functions with appropriate singular functions associated with a nodeless (unknown) variable [8], [9] which leads to an increase of the bandwidth of the global FEM matrix. The most efficient approach is the use of singular elements. In this case, the trial functions that are nonzero at the singular node are replaced with functions that properly model singular field behavior. Singular scalar elements have been used in various FEM formulations resulting in faster convergence of the numerical solution [10]–[12].

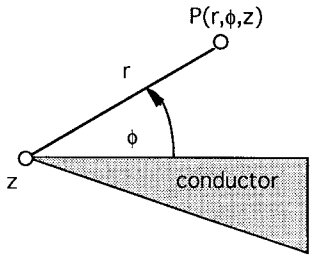

Fig. 1. Conducting edge embedded in a dielectric region.

In this paper, a new edge-based singular vector element similar to [13] is proposed. This singular vector element is compatible with the triangular-cell linear-tangential/quadratic-normal (LT/QN) edge element [14], and can cope with any order of singularity. Trial functions are expressed in a triangular polar coordinate system [15] and all the necessary integrations are performed analytically. The sparsity of the FEM equations is preserved, and spurious modes are eliminated. The number of unknown parameters needed to model the fields is significantly reduced by employing singular elements, as shown by numerical data. Results also suggest that for the same number of unknowns, the field distribution produced by the singular elements is much smoother in the vicinity of the singular point.

II. Basis-Function Definition

Our goal is to construct a vector trial function that can accurately model singular behavior near a sharp edge (Fig. 1) and at the same time be compatible with an ordinary curl-conforming element, i.e., require continuous tangential components and allow for discontinuous normal components along the element edges. Furthermore, the singular basis functions must not interfere with the interpolatory nature of the conventional LT/QN functions. The field in the vicinity of an edge behaves as [1], [2]

$$H_z = d_0 + r^{\nu} a_0(\varphi, z) + r^{\nu+1} a_1(\varphi, z) + r^{\nu+2} a_2(\varphi, z) + \cdots \tag{1a}$$

$$\bar{H}_t = r^{\nu-1} \bar{b}_0(\varphi, z) + r^{\nu} \bar{b}_1(\varphi, z) + r^{\nu+1} \bar{b}_2(\varphi, z) + \cdots \tag{1b}$$

Manuscript received March 25, 1997; revised November 21, 1997. This work was supported in part by the National Science Foundation under Grant ECS-9257927.

Z. Pantic-Tanner is with San Francisco State University, San Francisco, CA, 94132 USA.

J. S. Savage is with Ansoft Corporation, Pittsburgh, PA 15219 USA.

A. F. Peterson is with Georgia Institute of Technology, Atlanta, GA, 30332-0250 USA.

D. R. Tanner is with Lockheed Martin Corporation, Sunnyvale, CA 94088-3504 USA.

Publisher Item Identifier S 0018-9480(98)01594-4.

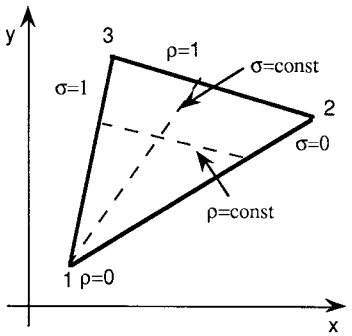

Fig. 2. Singular element with a triangular coordinate system.

where (r, ϕ, z) is the local polar coordinate system with the origin at the edge, as shown in Fig. 1. (We will use the magnetic field for illustration; the electric field can be modeled in a similar manner near an edge.) The singularity coefficient ν depends on the geometry and material properties [16]. Actually, only the transverse component is singular whereas the longitudinal component has a singular derivative.

To enhance the efficiency of the FEM, special singular elements can be created around an edge, replacing the ordinary cells of the FEM mesh. Fig. 2 depicts a singular element with local numbering of vertices denoted by 1, 2, and 3, with node 1 being the singular point on the edge. For convenience, we introduce a triangular polar coordinate system (ρ, σ) that is related to the (x, y) coordinates by [15]

$$x = x_1 + \rho[x_2 - x_1 + \sigma(x_3 - x_2)] \tag{2a}$$

$$y = y_1 + \rho[y_2 - y_1 + \sigma(y_3 - y_2)]. \tag{2b}$$

Hence, the H_z-field component can be expressed as

$$H_z = f_0 + \rho^\nu f_0(\sigma) + \rho^{\nu+1} f_1(\sigma) + \rho^{\nu+2} f_2(\sigma) + \cdots. \tag{3}$$

In order to model this behavior, the H_z-field within a singular element is expanded in terms of nodal-based coefficients Λ_{mn} and singular scalar basis functions B^M_{mn}, according to

$$H_z = \sum_{m=0}^{M} \sum_{n=0}^{m} \Lambda_{mn} B^M_{mn}(\rho, \sigma) \tag{4}$$

where

$$B^M_{mn}(\rho, \sigma) = R^M_m(\rho) L^m_n(\sigma) \tag{5}$$

and where the parameter M represents the order of singularity approximation in the radial direction. The distribution of nodes and the double indexing relationship (m, n) is shown in Fig. 3 for a second-order singular element.

The angular shape functions $L^m_n(\sigma)$ are the usual Lagrange polynomials

$$L^m_n(\sigma) = \prod_{\substack{j=0 \\ j \neq n}}^{m} \frac{m\sigma - j}{n - j}, \qquad n = 0, 1, \cdots, m. \tag{6}$$

The radial shape functions $R^M_m(\rho)$ represent the singular behavior in the radial direction

$$R^M_m(\rho) = \sum_{i=0}^{M} a_i \rho^{\nu+i-1} \tag{7a}$$

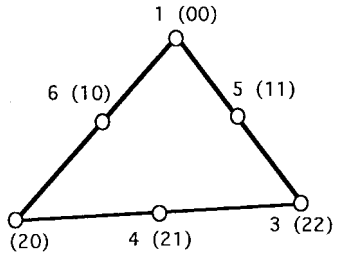

Fig. 3. Single and double node numbering for scalar B^M_{mn} basis functions in a second-order element.

and satisfy the conditions that $R^M_m(\rho)$ is zero at all nodes, except at the nodes where $i = m$:

$$\begin{aligned} R^M_m(i/M) &= 0, \qquad i = 1, 2, \cdots, m-1, m+1, \cdots, M \\ R^M_m(m/M) &= 1. \end{aligned} \tag{7b}$$

For example,

$$R^1_0(\rho) = 1 - \rho^\nu, R^1_1(\rho) = \rho^\nu \tag{8a}$$

$$\begin{aligned} R^2_0(\rho) &= 1 - (2^{\nu+1} - 1)\rho^\nu + (2^{\nu+1} - 2)\rho^{\nu+1} \\ R^2_1(\rho) &= 2^{\nu+1}\rho^\nu(1 - \rho) \\ R^2_2(\rho) &= -\rho^\nu(1 - 2\rho) \end{aligned} \tag{8b}$$

$$\begin{aligned} R^3_0(\rho) &= 1 - \left(1 + 3^{\nu+1} - \frac{3^{\nu+1}}{2^\nu}\right)\rho^\nu \\ &\quad + \left(\frac{9}{2} + \frac{5}{2}3^{\nu+1} - 4\frac{3^{\nu+1}}{2^\nu}\right)\rho^{\nu+1} \\ &\quad - \left(\frac{9}{2} + \frac{1}{2}3^{\nu+2} - \frac{3^{\nu+2}}{2^\nu}\right)\rho^{\nu+2} \\ R^3_1(\rho) &= \frac{3^{\nu+1}}{2}\rho^\nu(2 - 5\rho + 3\rho^2) \\ R^3_2(\rho) &= \frac{3^\nu}{2^\nu}\rho^\nu(3 - 12\rho + 9\rho^2) \\ R^3_3(\rho) &= \frac{1}{2}\rho^\nu(2 - 9\rho + 9\rho^2). \end{aligned} \tag{8c}$$

Note that the scalar singular functions B^M_{mn} are the same as those used in [12].

The transverse field H_t is expressed in terms of coefficients Ψ_i and edge-based vector basis functions $\bar{B}_i$ as

$$\bar{H}_t = \sum_{i=1}^{N} \Psi_i \bar{B}_i(\rho, \sigma) \tag{9}$$

where a few of the basis functions are singular and the rest of them nonsingular. In cases when the geometry of the waveguide or cavity cross section supports singular fields, the singular basis functions provide the proper dependence; if the actual fields are finite, the coefficients of the singular functions can vanish, allowing the nonsingular part of (9) to prevail.

The nonsingular basis functions are chosen to be the same as the ordinary LT/QN trial functions. The two LT/QN functions interpolating to nonzero tangential fields at the singular node are replaced by singular basis functions, which, according to Van Bladel [17] should be predominantly quasi-static in the vicinity of the edge. Hence, we construct each singular

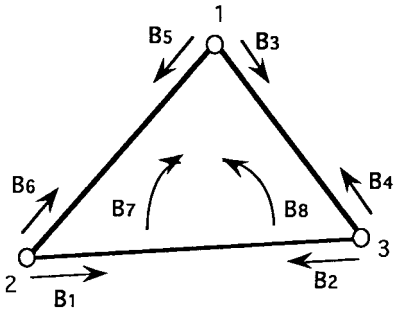

Fig. 4. Definition of vector basis functions in a second-order LT/QN edge element.

function as the gradient of a linear combination of nodal-based scalar functions B^M_{mn} (5) and a nonsingular part B_{kns}:

$$\begin{aligned}\bar{B}_k &= \bar{B}_{kns} + \sum_{mn} c_{kmn} \nabla_t B^M_{mn}(\rho,\sigma) \\ &= \bar{B}_{kns} + \sum_{mn} c_{kmn} \bar{B}^M_{mn}(\rho,\sigma) \end{aligned} \tag{10}$$

where the order of the singularity M is equal to the polynomial order of the tangential component in the neighboring edge elements

$$\begin{aligned}\bar{B}^M_{mn} =& \nabla_t B^M_{mn} \\ =& \frac{l_{23}\bar{n}_{23}}{2\Delta_e} \frac{\partial R^M_m(\rho)}{\partial \rho} L^m_n(\sigma) - \frac{l_{12}\bar{n}_{12}(1-\sigma)}{2\Delta_e \rho} \\ & \times R^M_m(\rho) \frac{\partial L^m_n(\sigma)}{\partial \sigma} + \frac{l_{31}\bar{n}_{31}\sigma}{2\Delta_e \rho} R^M_m(\rho) \frac{\partial L^m_n(\sigma)}{\partial \sigma} \end{aligned} \tag{11}$$

and $\bar{n}_{12}$, $\bar{n}_{23}$, and $\bar{n}_{31}$ are outward normals along edges 1–2, 2–3, and 3–1, respectively. The constants c_{kmn} and the nonsingular part $\bar{B}_{kns}$ in (10) are chosen in such way that the basis function $\bar{B}_k$ has a continuous tangential component along the edge it is associated with, and zero tangential components at the other two edges.

III. Singular Element Compatible With LT/QN Edge Element

In [14], an LT/QN edge element was derived for triangular cells based on the Nedelec conditions [18]. This element consists of eight vector basis functions, six edge-based and two face-based, as shown in Fig. 4. To generalize this type of element to the singular case, we choose two of the edge-based functions associated with singular node 1 (B_3 and B_5) to be singular, and the other six nonsingular. The entire set of eight functions can be expressed in the triangular polar coordinate system in the following way:

$$\bar{B}_1 = -\frac{l_{23}}{2\Delta_e} l_{12}\bar{n}_{12}\rho(1-\sigma) \tag{12a}$$

$$\bar{B}_2 = -\frac{l_{23}}{2\Delta_e} l_{31}\bar{n}_{31}\rho\sigma \tag{12b}$$

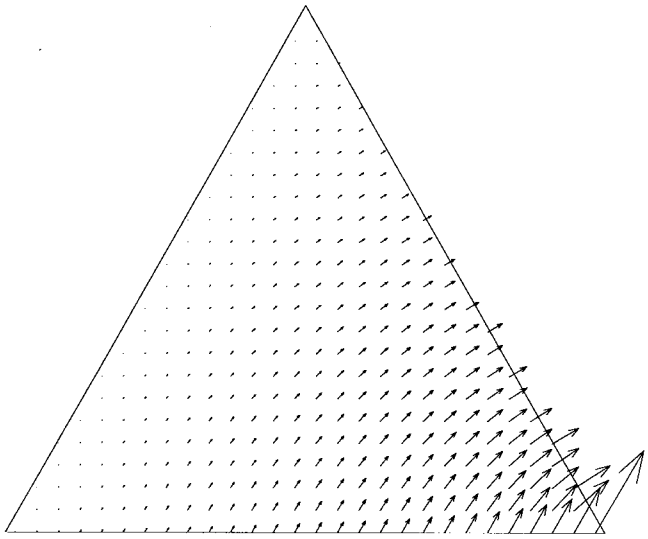

Fig. 5. Edge-based singular vector basis function.

$$\begin{aligned}\bar{B}_3 = \nabla_t B^1_{11} + \bar{B}_{3ns} =& \frac{l_{23}\bar{n}_{23}}{2\Delta_e}\nu(\rho^{\nu-1} - \rho)\sigma \\ & - \frac{l_{12}\bar{n}_{12}}{2\Delta_e}(\rho^{\nu-1} - \rho)(1-\sigma) + \frac{l_{31}\bar{n}_{31}}{2\Delta_e}(\rho^{\nu-1} - \rho)\sigma \end{aligned} \tag{12c}$$

$$\bar{B}_4 = -\frac{l_{31}}{2\Delta_e} l_{23}\bar{n}_{23}\rho\sigma \tag{12d}$$

$$\begin{aligned}\bar{B}_5 = \nabla_t B^1_{10} + \bar{B}_{5ns} =& \frac{l_{23}\bar{n}_{23}}{2\Delta_e}\nu(\rho^{\nu-1} - \rho)(1-\sigma) \\ & + \frac{l_{12}\bar{n}_{12}}{2\Delta_e}(\rho^{\nu-1} - \rho)(1-\sigma) - \frac{l_{31}\bar{n}_{31}}{2\Delta_e}(\rho^{\nu-1} - \rho)\sigma \end{aligned} \tag{12e}$$

$$\bar{B}_6 = -\frac{l_{12}}{2\Delta_e} l_{23}\bar{n}_{23}\rho(1-\sigma) \tag{12f}$$

$$\bar{B}_7 = \frac{l_{12}\bar{n}_{12}}{2\Delta_e}\rho(1-\rho)(1-\sigma) - \frac{l_{31}\bar{n}_{31}}{2\Delta_e}\rho(1-\rho)\sigma \tag{12g}$$

$$\bar{B}_8 = \frac{l_{23}\bar{n}_{23}}{2\Delta_e}\rho^2\sigma(1-\sigma) - \frac{l_{31}\bar{n}_{31}}{2\Delta_e}\rho(1-\rho)\sigma. \tag{12h}$$

A plot of a singular basis function is shown in Fig. 5. (The nonsingular functions are plotted in [14].) Cell-to-cell continuity conditions are imposed so that the representation produces continuous tangential components throughout the mesh, but permits discontinuous normal components between cells in common with the conventional LT/QN functions.

IV. Application to Resonant Cavity Analysis

To illustrate relative accuracy, the LT/QN-compatible singular elements were used to estimate the wavenumbers $k = \omega\sqrt{\varepsilon\mu}$ of the transverse vector Helmholtz equation

$$\nabla_t \times (\nabla_t \times \bar{H}_t) = k^2 \bar{H}_t \tag{13}$$

for several two-dimensional (2-D) cavity problems involving homogeneous media with permittivity ε_0 and permeability μ_0. After applying the Galerkin procedure, a generalized matrix eigenvalue equation $Ee = k^2 Fe$ is obtained. The required

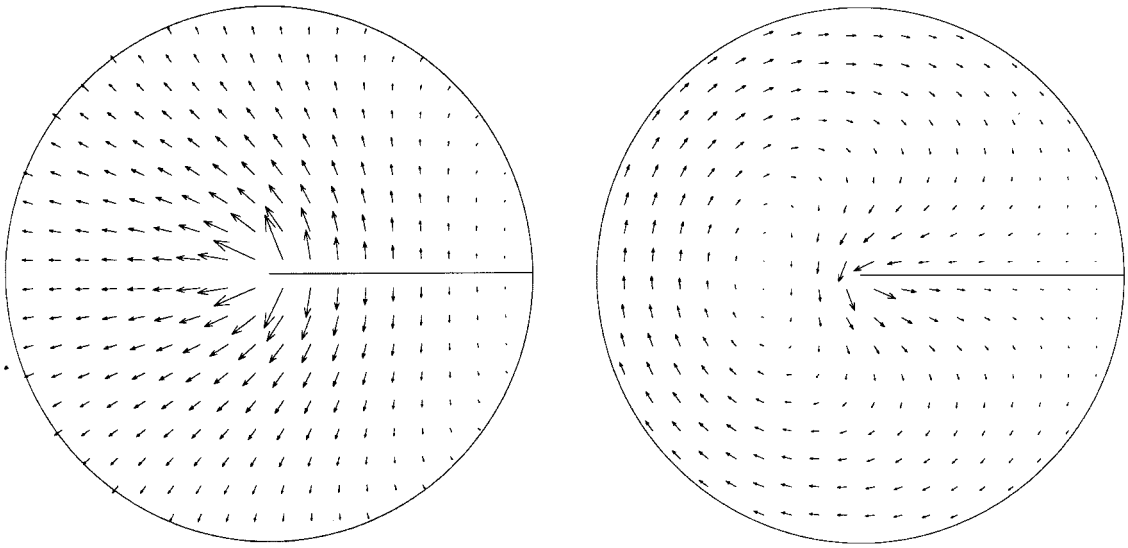

(a) (b)

Fig. 6. (a) The TE field associated with the lowest order electric mode. (b) The magnetic field associated with the lowest order TM mode.

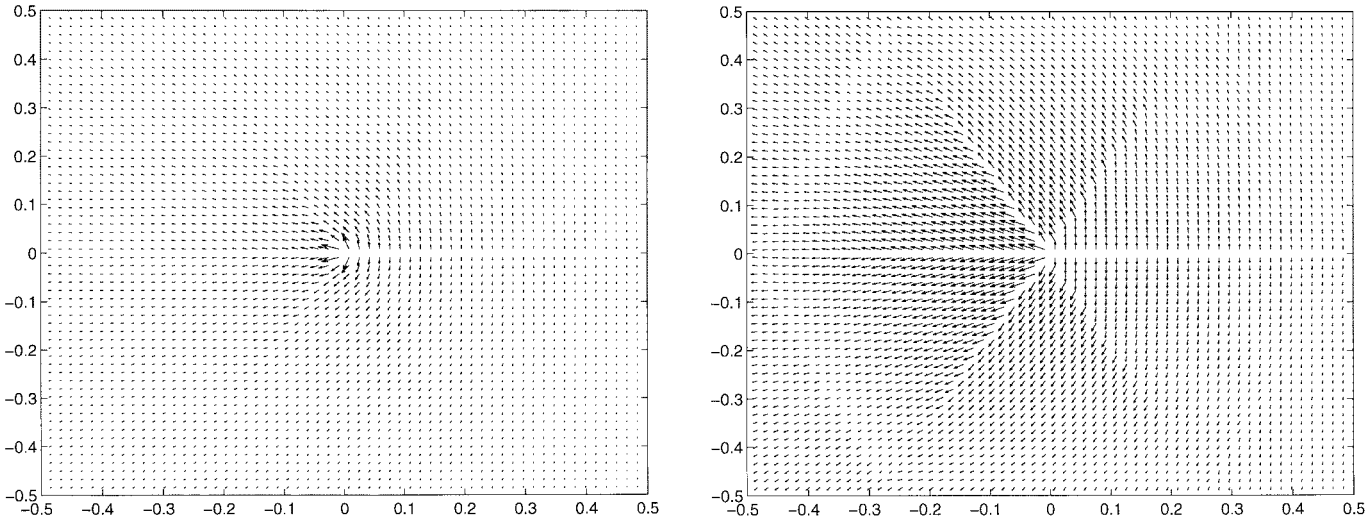

(a) (b)

Fig. 7. An expanded view of the electric field in the immediate vicinity of the baffle tip. (a) Electric field obtained using singular elements in the cells adjacent to the tip. (b) Electric field obtained using only nonsingular LT/QN functions throughout the mesh.

element matrices are

$$E_{ij} = \iint_{\Delta_e} \{(\nabla_t \times \bar{B}_i) \cdot (\nabla_t \times \bar{B}_j)\}\, dS \tag{14}$$

and

$$F_{ij} = \iint_{\Delta_e} \{\bar{B}_i \cdot \bar{B}_j\}\, dS \tag{15}$$

where Δ_e is the area of the element. Since the basis functions B_i are given in the triangular coordinate system (ρ, σ), all integrations involve polynomial products and can be evaluated analytically. This eigenvalue problem is solved iteratively, taking advantage of the sparsity of the global FEM matrices [19]. The above equations describe the TM modes of a 2-D cavity; the TE modes can be obtained from (13) by exchanging the magnetic field with the electric field and imposing the essential boundary condition that the tangential electric field vanishes on a perfect conductor.

Consider a homogeneous circular cavity of unit radius with a baffle extending to the center (Fig. 6) for which the 2-D modes and resonant frequencies can be found analytically. Fig. 6(a) shows the electric field for the lowest order TE mode, while Fig. 6(b) shows the magnetic field for the lowest order TM mode. Both appear to exhibit a singularity at the baffle tip. These results were obtained by representing the electric field with ordinary LT/QN elements everywhere, except in the cells adjacent to the tip of the baffle, where they were replaced by the singular functions of (12). Fig. 7(a) shows an expanded view of the TE field in the immediate vicinity of the edge obtained using the singular functions, while Fig. 7(b)

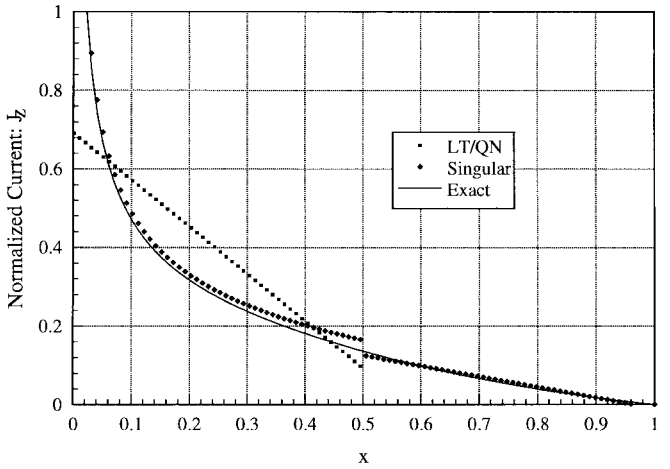

Fig. 8. Normalized surface current on the baffle of the circular cavity for a coarse mesh with only two edges on the baffle. The result using an LT/QN expansion is compared to that obtained with singular basis functions around the tip of the baffle and to the exact solution.

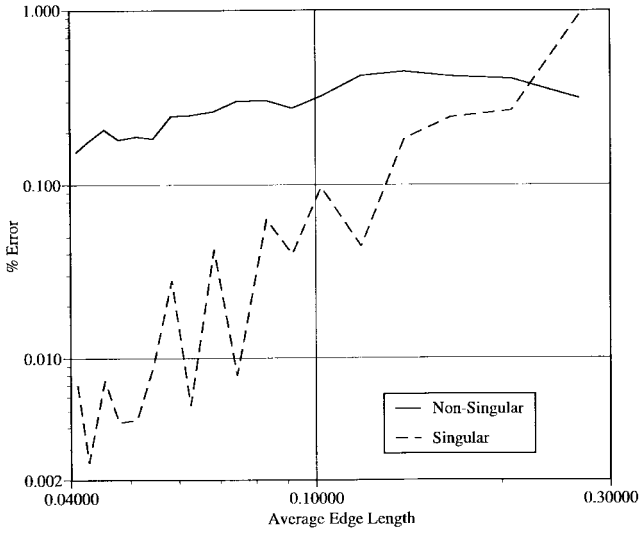

Fig. 9. Error in the lowest order TM wavenumber versus average edge length in the mesh for 18 unstructured triangular-cell meshes. This mode has a singularity at the baffle tip, and results obtained using ordinary LT/QN elements everywhere are compared with results from LT/QN elements augmented with singular elements around the tip.

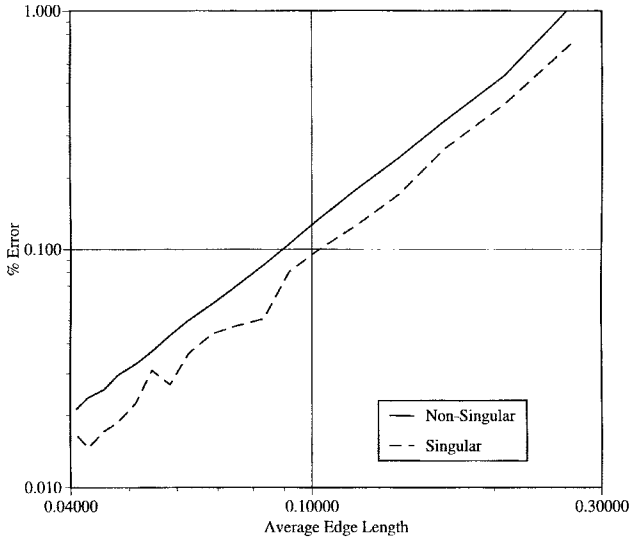

Fig. 10. Error in the second TM wavenumber versus average edge length in the mesh for the same meshes used to produce Fig. 8. This mode is nonsingular, but illustration results obtained using ordinary LT/QN elements everywhere are compared with results from LT/QN elements augmented with singular elements around the tip.

TABLE I
LOWEST TE WAVENUMBER FOR THE L-SHAPED CAVITY, PRODUCED BY VARIOUS TRIANGULAR-CELL MESHES WITH AVERAGE EDGE LENGTH INDICATED. THIS IS A SINGULAR MODE, AND RESULTS OBTAINED WITH SINGULAR ELEMENTS AROUND THE CORNER ARE COMPARED WITH RESULTS OBTAINED USING ONLY NONSINGULAR LT/QN ELEMENTS THROUGHOUT THE MESH

edge length	non-singular	singular
1.360	1.160	1.192
0.840	1.199	1.214
0.556	1.205	1.214
0.412	1.209	1.214
0.281	1.211	1.214
0.203	1.212	1.215
0.141	1.213	1.215
0.101	1.214	1.215
0.071	1.214	1.215
0.050	1.214	1.215
0.036	1.214	1.215
0.025	1.214	1.215

shows the identical view for the TE mode obtained using only the nonsingular LT/QN elements. It is apparent from Fig. 7 that the singular elements produce a smoother less distorted field plot in the vicinity of the singularity. Fig. 8 shows a comparison of the exact and numerical results for the TM surface current on the baffle for a coarse mesh with only two edges along the baffle. The singular basis function closely tracks the exact singularity. To illustrate convergence, Fig. 9 shows the error in the eigenvalue associated with the lowest order TM mode versus average edge length in the mesh for singular and nonsingular basis functions. Data were obtained using 18 unstructured triangular-cell meshes; the finest mesh produces about 22 000 unknowns. Fig. 10 shows similar data for the next higher TM mode, which is nonsingular. Results obtained using the singular basis functions show much steeper convergence curves than the nonsingular basis functions for the singular modes; for the nonsingular modes the error curves are similar whether singular or nonsingular basis functions are used. All computations were done in single precision, and produced at least four significant digits after eigensolution. The observed convergence behavior for TE modes is similar.

As a second example, consider an L-shaped cavity with exterior dimensions 2×2, and the interior corner located at the center. Fig. 11(a) shows a vector plot of the lowest order TE mode, while Fig. 11(b) shows the lowest order TM mode. Both are singular at the interior corner. Table I shows numerical results for the lowest order TE eigenvalue as a function of average edge length in the various finite-element meshes used to represent the region. The results obtained using singular functions at the corner appear to converge much faster than the results obtained using ordinary LT/QN elements everywhere. Similar convergence rates were observed for the lowest order

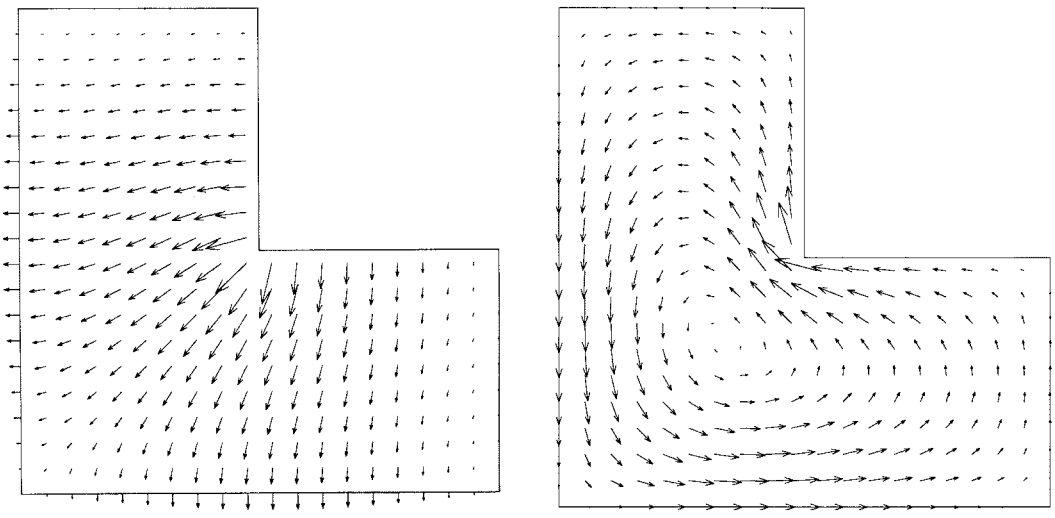

(a) (b)

Fig. 11. (a) The electric field associated with the lowest order TE mode. (b) The magnetic field associated with the lowest order TM mode.

TABLE II
SECOND TE WAVENUMBER FOR THE L-SHAPED CAVITY, PRODUCED BY VARIOUS TRIANGULAR-CELL MESHES WITH AVERAGE EDGE LENGTH INDICATED. THIS IS A NONSINGULAR MODE, AND RESULTS OBTAINED WITH SINGULAR ELEMENTS AROUND THE CORNER ARE COMPARED WITH RESULTS OBTAINED USING ONLY NONSINGULAR LT/QN ELEMENTS THROUGHOUT THE MESH

edge length	non-singular	singular
1.360	1.868	1.825
0.840	1.878	1.867
0.556	1.879	1.874
0.412	1.880	1.878
0.281	1.880	1.879
0.203	1.880	1.880
0.141	1.880	1.880
0.101	1.880	1.880
0.071	1.880	1.880
0.050	1.880	1.880
0.036	1.880	1.880
0.025	1.880	1.880

TM mode. Table II shows numerical results obtained for the next higher TE mode, which is finite at the corner. For this nonsingular mode, the error produced using the singular functions in the vicinity of the edge is not much different from the error produced without the singular functions present, although it is slightly greater for coarse meshes.

V. CONCLUSION

A new singular vector finite element compatible with LT/QN edge-elements has been developed. It provides continuous tangential and discontinuous normal components along the element edges. Out of eight basis functions per triangle, six edge-based and two face-based, two are chosen to be singular in accordance with Van Bladel's prescription [17]. The other six functions are nonsingular and the same as ordinary LT/QN elements.

Two types of homogeneous cavity structures have been analyzed for illustration. For singular cavity modes, the singular elements provide improved convergence, and smoother fields in the cells near the corner or edge. Consequently, they offer improved accuracy with far fewer unknowns. For nonsingular modes, the use of singular elements increases the observed error only slightly, and does not appear to affect the rate of convergence. Thus, the singular elements can be used in locations where a field singularity is expected. If such a singularity is absent, the results will not be adversely affected.

REFERENCES

[1] J. Meixner, "The behavior of electromagnetic fields at edges," *IEEE Trans. Antennas Propagat.*, vol. AP-20, pp. 442–446, July 1972.
[2] J. V. Bladel, *Singular Electromagnetic Fields and Sources* (Oxford Engineering Science Series 28). Oxford, U.K.: Clarendon, 1991.
[3] P. Daly, "Singularities in transmission lines," in *The Mathematics of Finite Elements and Applications*, J. R. Whiteman, Ed.. New York: Academic, 1973, pp. 337–350.
[4] Z. J. Cendes, D. N. Shenton, and H. Shahnasser, "Magnetic field computation using Delaney triangulation and complementary finite element methods," *IEEE Trans. Magn.*, vol. MAG-19, pp. 2251–2554, Nov. 1983.
[5] R. Miniowitz and J. P. Webb, "Covariant-projection quadrilateral elements for the analysis of waveguides with sharp edges," *IEEE Trans. Microwave Theory Tech.*, vol. 39, pp. 501–505, Mar. 1991.
[6] K. Ise, K. Inoue, and M. Koshiba, "Three-dimensional finite-element method with edge elements for electromagnetic waveguides discontinuities," *IEEE Trans. Microwave Theory Tech.*, vol. 39, pp. 1289–1295, Aug. 1991.
[7] J. F. Lee, D. K. Sun, and Z. J. Cendes, "Full-wave analysis of dielectric waveguides using tangential vector finite elements," *IEEE Trans. Microwave Theory Tech.*, vol. 39, pp. 1262–1271, Aug. 1991.
[8] J. R. Whiteman, "Finite elements, singularities and fracture," in *The Mathematics of Finite Elements and Applications III, MAFELAP 1978*, J. R. Whiteman, Ed. New York: Academic, 1979, pp. 35–54.
[9] J. P. Webb, "Finite element analysis of dispersion in waveguides with sharp metal edges," *IEEE Trans. Microwave Theory Tech.*, vol. 36, pp. 1819–1824, Dec. 1988.
[10] Z. Pantic and R. Mittra, "Quasi-TEM analysis of microwave transmission lines by the finite-element method," *IEEE Trans. Microwave Theory Tech.*, vol. MTT-34, pp. 1096–1103, Nov. 1986.
[11] J. M. Gill and J. Zapata, "Efficient singular element for finite element analysis of quasi-TEM transmission lines and waveguides with sharp metal edges," *IEEE Trans. Microwave Theory Tech.*, vol. 42, pp. 92–98, Jan. 1994.
[12] Z. Pantic-Tanner, C. H. Chan, and R. Mittra, "The treatment of edge singularities in the full-wave finite element solution of waveguiding problems," in *URSI Symp. Dig.*, Syracuse, NY, June 1988, p. 336.
[13] Z. Pantic-Tanner, D. R. Tanner, S. A. Savage, and A. F. Peterson, "The treatment of edge singularities in waveguiding problems using a finite element method based on edge elements," in *URSI Symp. Dig.*, Newport Beach, CA, June 1995, p. 90.

[14] A. F. Peterson, "Vector finite element formulation for scattering from two-dimensional heterogeneous bodies," *IEEE Trans. Antennas Propagat.*, vol. 43, pp. 357–365, Mar. 1994.
[15] M. Stern and E. B. Becker, "A conforming crack tip element with quadratic variation in the singular fields," *Int. J. Numer. Methods Eng.*, vol. 12, pp. 279–288, 1978.
[16] C. H. Chan, Z. Pantic-Tanner, and R. Mittra, "Field behavior near a conducting edge embedded in an inhomogeneous anisotropic medium," *Electron. Lett.*, vol. 24, pp. 355–356, 1988.
[17] J. V. Bladel, "Field singularities at metal-dielectric wedges," *IEEE Trans. Antennas Propagat.*, vol. AP-33, pp. 450–455, Apr. 1985.
[18] J. C. Nedelec, "Mixed finite elements in R3," *Numer. Math.*, vol. 35, pp. 315–341, 1980.
[19] J. S. Savage and A. F. Peterson, "Higher-order vector finite elements for tetrahedral cells," *IEEE Trans. Microwave Theory Tech.*, vol. 44, pp. 874–879, June 1996.

Zorica Pantic-Tanner received the B.S., M.S., and Ph.D. degrees in electrical engineering from the University of Nish, Nish, Yugoslavia, in 1975, 1978, and 1982, respectively.

From 1984 to 1989, she worked in the Electromagnetic Communications Laboratory, University of Illinois at Urbana-Champaign, first as a Fulbright Post-Doctoral Fellow, and then as a Visiting Scientist. In 1989, she joined the School of Engineering, San Francisco State University, San Francisco, CA, as an Associate Professor, and became a Full Professor in 1996. She is currently Director of the School of Engineering, San Francisco State University. Her research interests are in the areas of numerical modeling, applied electromagnetics, and electromagnetic compatibility.

Dr. Pantic-Tanner is a member of the International EMC Education Committee, treasurer of the Santa Clara Valley Chapter of the IEEE EMC Society, and the vice-chair of the International EMC Numerical Modeling Committee.

J. Scott Savage (S'95) received the B.E.E. degree from the Georgia Institute of Technology, in 1992, the M.S.E.E. degree from the University of Kentucky, Lexington, in 1993, and the Ph.D. degree from the Georgia Institute of Technology, Atlanta, in 1997.

From 1992 to 1993, he was a Research Assistant studying crosstalk in cable bundles with Ford Motor Company. From 1994 to 1997, he was a Research Assistant at the Georgia Institute of Technology. He is currently with Ansoft Coporation, Pittsburgh, PA. His interests include computational and applied electromagnetics.

Mr. Savage is a member of Eta Kappa Nu and Tau Beta Pi.

David R. Tanner (S'82–M'85), photograph and biography not available at the time of publication.

Andrew F. Peterson (S'82–M'83–SM'92) received the B.S., M.S., and Ph.D. degrees in electrical engineering from the University of Illinois at Urbana-Champaign, in 1982, 1983, and 1986, respectively.

Since 1989, he has been a Faculty Member of the School of Electrical and Computer Engineering, Georgia Institute of Technology, Atlanta, where he is currently an Assistant Professor teaching electromagnetic-field theory and computational electromagnetics, and conducting research in the development of computational techniques for electromagnetic scattering, microwave devices, and electronic packaging applications.

Dr. Peterson is a member of URSI Commission B, ASEE, and AAUP. He has served as an associate editor of the IEEE TRANSACTIONS ON ANTENNAS AND PROPAGATION, chairman of the Atlanta joint IEEE AP-S/MTT chapter, and is currently the general chair of the 1998 IEEE AP-S International Symposium and URSI National Radio Science Meeting, Atlanta, GA. He has also served for six years as a director of ACES.